

Volume-Preserving Transformers for Learning Time Series Data with Structure

Benedikt Brantner¹, Guillaume de Romemont^{2,3}, Michael Kraus¹, and Zeyuan Li⁴

¹*Max-Planck-Institut für Plasmaphysik, Boltzmannstraße 2, 85748 Garching*

²*DAAA, ONERA, Université Paris Saclay, F-92322, Châtillon, France*

³*Arts et Métiers Institute of Technology, Paris, France*

⁴*Zentrum Mathematik, Technische Universität München, Boltzmannstraße 3, 85748 Garching, Germany*

May 2, 2024

Abstract. Two of the many trends in neural network research of the past few years have been (i) the learning of dynamical systems, especially with recurrent neural networks such as long short-term memory networks (LSTMs) and (ii) the introduction of transformer neural networks for natural language processing (NLP) tasks. Both of these trends have created enormous amounts of traction, particularly the second one: transformer networks now dominate the field of NLP.

Even though some work has been performed on the intersection of these two trends, those efforts were largely limited to using the vanilla transformer directly without adjusting its architecture for the setting of a physical system.

In this work we use a transformer-inspired neural network to learn a dynamical system and furthermore (for the first time) imbue it with structure-preserving properties to improve long-term stability. This is shown to be of great advantage when applying the neural network to real world applications.

Résumé. Deux des nombreuses tendances de la recherche sur les réseaux neuronaux de ces dernières années ont été (i) l'apprentissage des systèmes dynamiques, en particulier avec les réseaux neuronaux récurrents tels que les Long Short Term Memory (LSTM) et (ii) l'introduction de réseaux neuronaux transformer pour le traitement du langage naturel (NLP). Ces deux tendances ont suscité un énorme engouement, en particulier la seconde : les réseaux transformer dominent désormais le NLP.

Bien que certains travaux aient été réalisés à l'intersection de ces deux tendances, ils se sont largement limités à l'utilisation directe du transformer vanilla sans adapter son architecture à la configuration d'un système physique.

Dans ce cadre, nous utilisons un réseau neuronal inspiré d'un transformer pour apprendre un système dynamique et, en outre (pour la première fois), lui conférer des propriétés de préservation de la structure afin d'améliorer la stabilité à long terme. Ces propriétés s'avèrent extrêmement importantes lors de l'application du réseau neuronal à des applications réelles.

Keywords: Reduced-Order Modeling, Hyper Reduction, Machine Learning, Transformers, Neural Networks, Divergence-Free, Volume-Preserving, Structure-Preserving, Multi-Step Methods

Introduction

This work is concerned with the development of accurate and robust neural network architectures for the solution of differential equations. It is motivated by several trends that have determined the focus of research in scientific machine learning [1] in recent years.

First, machine learning techniques have been successfully applied to the identification of dynamical systems for which data are available, but the underlying differential equation is either (i) not known or (ii) too expensive to solve. The first problem (i) often occurs when dealing with experimental data [2, 3]; the second one (ii) is crucial in *reduced-order modeling* as will be elaborated on below. Various machine learning models have been shown to be able to capture the behaviour of dynamical systems accurately and (within their regime of validity) make predictions at much lower computational costs than traditional numerical algorithms.

Second, in certain application areas, hitherto established neural network architectures have been gradually replaced by transformer neural networks [4]. Primarily, this concerns recurrent neural networks such as long short-term memory networks (LSTMs [5]) that treat time series data, e.g., for natural language processing, but also convolutional neural networks (CNNs) for image recognition [6]. Transformer networks tend to capture long-range dependencies and contextual information better than other architectures and allow for much more efficient parallelization on modern hardware.

Lastly, the importance of including information about the physical system into scientific machine learning models has been recognized. This did not come as a surprise as it is a finding that had long been established for conventional numerical methods [7]. In this work, the physical property we consider is *volume preservation* [7, 8], which is a property of the flow of divergence-free vector fields. There are essentially two approaches through which this property can be accounted for: the first one is the inclusion of terms in the loss function that penalize non-physical behaviour; these neural networks are known as physics-informed neural networks (PINNs¹ [9]). The drawback of this approach is that a given property is enforced only weakly and therefore only approximately satisfied. The other approach, and the one taken here, is to encode physical properties into the network architecture; a related example of this are “symplectic neural networks” (SympNets [10]). While this approach is often more challenging to implement, the resulting architectures adhere to a given property exactly.

An application, where all of these developments intersect, is *reduced-order modeling* [12–14], which is used in the following setting: Suppose we are given a high-dimensional parametric ordinary differential equation (PODE), referred to as the full order model (FOM), obtained from discretizing a parametric partial differential equation (PPDE). Typically the high-dimensional PODE needs to be solved for many different parameter instances [12, 14], resulting in prohibitively expensive computational costs. In order to alleviate the computational cost involved in solving the high-dimensional PODE many times, a reduced model is built based on training data. A typical reduced-order modeling framework consists of three stages:

1. Solving the FOM for a limited range of parameter values to obtain *training data*.
2. Constructing two maps, called *reduction* and *reconstruction*, that map from the FOM space to a reduced space of much smaller dimension and from this reduced space to the FOM space respectively. This is referred to as the *offline stage*.
3. Solving the reduced model. This is a PODE of much smaller dimension. This step is referred as the *online stage*.

In this work, we are concerned with the third step in this framework, the *online stage*. Our aim is to construct structure-preserving neural network models, that can be used to compute the dynamics of reduced models. Efforts to use neural networks for the online stage have been made in the past, for example using LSTMs [13, 14].² Inspired by one of the trends mentioned above, namely the gradual replacement of such architectures, our work will be based on transformers instead.

While previously, other authors applied transformers for model reduction, and volume-preserving neural networks have been developed as well, both aspect have not yet been considered together. Thus

¹See [11] for an application of PINNs where *non-physical behavior* is penalized.

²Apart from neural networks, there are also other approaches to alleviate the cost during the online stage, notably the “discrete empirical interpolation method” (DEIM [15]).

to our knowledge, this work is the first that aims at imbuing a transformer with structure-preserving properties (namely volume-preservation) and applying it to a system described by a divergence-free vector field. Specifically, transformer neural networks have been used for the online stage in reduced order modeling in [16, 17]. The authors applied the vanilla transformer architecture without taking any physical properties of the system into account. Volume-preserving feed-forward neural networks have been developed in [18]. The authors based the network design on a theorem introduced in [19] for the design of traditional integrators for divergence-free vector fields [7].

The remainder of this paper is structured as follows: In Section 1 we discuss the basic theory behind divergence-free vector fields and volume-preserving flows, in Section 2 the (standard) transformer is introduced, in Section 3 we introduce a new class of volume-preserving feedforward neural networks (that differ slightly from what is discussed in e.g. [18]), in Section 4 we introduce our new adapted transformer, in Appendix A we discuss the rigid body as an example of a system described by a divergence-free vector field and in Section 5 we finally present experimental results. In Section 6 we summarize our findings and state potential future investigations to extend the work presented here.

1 Divergence-free vector fields

The aim of this work is to adapt the transformer architecture to the setting of dynamical systems that are described by *divergence-free vector fields* on \mathbb{R}^d , i.e. mappings $f : \mathbb{R}^d \rightarrow \mathbb{R}^d$ for which $\nabla \cdot f = \sum_i \partial_i f_i = 0$. The *flow* of such a vector field f is the (unique) map $\varphi_f^t : \mathbb{R}^d \rightarrow \mathbb{R}^d$, such that

$$\left. \frac{d}{dt} \right|_{t=t_0} \varphi^t(z) = f(\varphi^{t_0}(z)), \quad (1)$$

for $z \in \mathbb{R}^d$ and t is a time step. For a divergence-free vector field f the flow φ_f^t is volume-preserving, i.e. the determinant of the Jacobian of φ_f^t is one: $\det(\nabla \varphi_f^t) = 1$. This can easily be proved:

$$\frac{d}{dt} \nabla \varphi^t(z) = \nabla f(\varphi^t(z)) \nabla \varphi^t(z) \implies \text{tr} \left((\nabla \varphi^t(z))^{-1} \frac{d}{dt} \nabla \varphi^t(z) \right) = \text{tr} (\nabla f(\varphi^t(z))) = 0. \quad (2)$$

We further have

$$\text{tr}(A^{-1} \dot{A}) = \frac{\frac{d}{dt} \det(A)}{\det(A)} \quad (3)$$

and therefore

$$\frac{d}{dt} \det(\nabla \varphi^t(z)) = 0. \quad (4)$$

In Equation (2) we have also used that the flow of the ODE is invertible.

Numerical integrators for ODEs constitute an approximation ψ^h of the flow φ_f^t where h denotes the time step, which most of the time is fixed. If the flow φ_f^t exhibits certain properties (like volume preservation) it appears natural to also imbue ψ^h with these properties. The discipline of doing so is generally known as *geometric numerical integration* [7, 20].

In recent years, numerical integrators based on neural networks have emerged and it has proven crucial to also imbue these integrators with properties of the system such as symplecticity [10, 21] and volume preservation [18]. The neural network architecture presented in Section 4 falls in this category.

Let us note that all symplectic and Hamiltonian vector fields³ are also divergence-free but not vice-versa. Symplecticity is a much stronger property than volume preservation. Therefore, preserving symplecticity is often preferable to preserving volume. Still, volume preservation usually offers improved stability and robustness over schemes that do not respect any of the properties of the vector field. Thus, volume-preserving methods can be a viable option when symplectic schemes are not available.

³Strictly speaking Hamiltonian vector fields form a subspace of the space of all symplectic vector fields (see [22]).

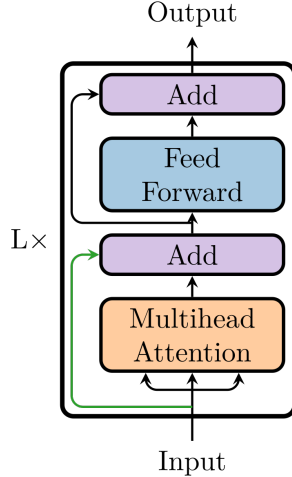


Figure 1: Sketch of the transformer architecture. It is a composition of an attention layer and a feedforward neural network. The first *add connection* is drawn in light green to emphasize that this can be left out.

2 The transformer

The transformer architecture [4] was originally motivated by natural language processing (NLP) tasks and has quickly come to dominate that field. The “T” in ChatGPT (see e.g. [23]) stands for “Transformer” and transformer models are the key element for generative AI. These models are a type of neural network architecture designed to process sequential input data, such as sentences or time-series data. The transformer has replaced, or is in the process of replacing, earlier architectures such as long short term memory (LSTM) networks [24] and other recurrent neural networks (RNNs, see [25]). The transformer architecture is visualized in Figure 1⁴.

In essence, the transformer consists of an attention layer (explained below) and a residual network (ResNet⁵ [26]). Despite its simplicity, the transformer exhibits vast improvements compared to RNNs and LSTMs, including the ability to better capture long-range dependencies and contextual information and its near-perfect parallelizability for computation on GPUs and modern hardware. Furthermore, the simplicity of the transformer architecture makes it possible to interpret all its constituent operations, which is not so much the case with LSTMs, for example. As the individual operations have a straightforward mathematical interpretation, it is easier to imbue them with additional structure such as volume-preservation.

The attention layer, the first part of a transformer layer, takes a series of vectors $z_\mu^{(1)}, \dots, z_\mu^{(T)}$ as input (the μ indicates a specific time sequence) and outputs a *learned convex combination of these vectors*. So for a specific input:

$$input = [z_\mu^{(1)}, z_\mu^{(2)}, \dots, z_\mu^{(T)}], \quad (5)$$

the output of an attention layer becomes:

$$output = \left[\sum_{i=1}^T y_i^{(1)} z_\mu^{(i)}, \sum_{i=1}^T y_i^{(2)} z_\mu^{(i)}, \dots, \sum_{i=1}^T y_i^{(T)} z_\mu^{(i)} \right], \quad (6)$$

⁴The three arrows going into the multihead attention module symbolize that the input is used three times: twice when computing the correlation matrix C and then again when the input is re-weighted based on C . In the NLP literature those inputs are referred to as “queries”, “keys” and “values” [4].

⁵The simplest form of a ResNet is a regular feed-forward neural network with an add connection: $x \rightarrow x + \sigma(Wx + b)$. In this work we use a slightly more complicated version where the ResNet step is repeated `n_blocks` times (also confer Figure 2).

with the coefficients $y_i^{(j)}$ satisfying $\sum_{i=1}^T y_i^{(j)} = 1 \forall j = 1, \dots, T$. It is important to note that the mapping

$$\text{input} \mapsto ([y_i^{(j)}]_{i=1, \dots, T, j=1, \dots, T}) \quad (7)$$

is nonlinear. These coefficients are computed based on a correlation of the input data and involve learnable parameters that are adapted to the data during training.

The correlations in the input data are computed through a *correlation matrix* $: Z \rightarrow Z^T A Z =: C$; they are therefore determined by computing weighted scalar products of all possible combinations of two input vectors where the weighting is done with A ; any entry of the matrix $c_{ij} = (z_\mu^{(i)})^T A z_\mu^{(j)}$ is the result of computing the scalar product of two input vectors. So any relationship, short-term or long-term, is encoded in this matrix.

In the next step, a softmax function is applied column-wise to C and returns the following output:

$$y_i^{(j)} = [\text{softmax}(C)]_{ij} := e^{c_{ij}} / \left(\sum_{i'=1}^T e^{c_{i'j}} \right). \quad (8)$$

This softmax function maps the correlation matrix to a sequence of *probability vectors*, i.e., vectors in the space $\mathcal{P} := \{\mathbf{y} \in [0, 1]^d : \sum_{i=1}^d y_i = 1\}$. Every one of these d probability vectors is then used to compute a convex combination of the input vectors $[z_\mu^{(1)}, z_\mu^{(2)}, \dots, z_\mu^{(T)}]$, i.e., we get $\sum_{i=1}^T y_i^{(j)} z_\mu^{(i)}$ for $j = 1, \dots, T$.

Remark 1 *Figure 1 indicates the use of a multi-head attention layer as opposed to a single-head attention layer. What we described in this section is single-head attention. A multi-head attention layer is slightly more complex: it is a concatenation of multiple single-head attention layers. This is useful for NLP tasks⁶, but introduces additional complexity that makes it harder to imbue the multi-head attention layer with structure-preserving properties.*

3 Volume-preserving feedforward neural networks

As a first step to construct a *structure-preserving transformer* we replace the ResNet in the transformer with a feedforward neural network that is volume-preserving. The *volume-preserving feedforward layers* here are inspired by the linear and activation modules from [10]. The key ingredients are upper-triangular matrices U and lower-triangular matrices L , whose components are such that $u_{ij} = 0$ if $i \geq j$ and $l_{ij} = 0$ if $i \leq j$, respectively.

Let us consider a “lower-triangular layer”:

$$x \mapsto x + \sigma(Lx + b), \quad (9)$$

with the matrix L given by:

$$L = \begin{pmatrix} 0 & 0 & \cdots & 0 \\ a_{21} & \ddots & & \vdots \\ \vdots & \ddots & \ddots & \vdots \\ a_{n1} & \cdots & a_{n(n-1)} & 0 \end{pmatrix}. \quad (10)$$

The Jacobian of such a layer is of the form

⁶Intuitively, multi-head attention layers allow for attending to different parts of the sequence in different ways (i.e. different heads in the multi-head attention layer *attend to* different parts of the input sequence) and can therefore extract richer contextual information.

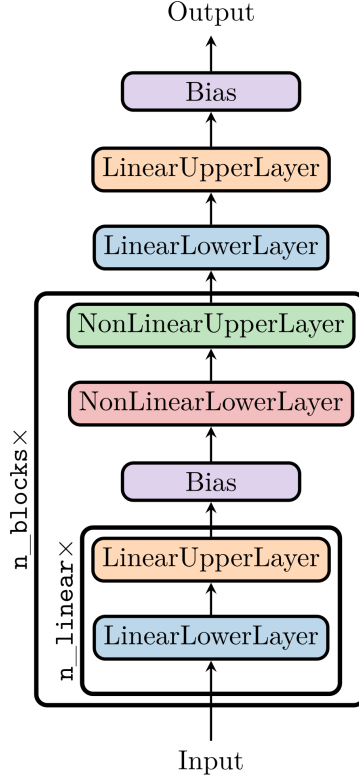


Figure 2: Architecture of the volume-preserving feedforward neural network. “LinearLowerLayer” refers to $x \mapsto x + Lx$ (and similarly for “LinearUpperLayer”). “NonLinearLowerLayer” is shown in Equation (9). “Bias” is the addition with a bias vector.

$$J = \begin{pmatrix} 1 & 0 & \cdots & 0 \\ b_{21} & \ddots & & \vdots \\ \vdots & \ddots & \ddots & \vdots \\ b_{n1} & \cdots & b_{n(n-1)} & 1 \end{pmatrix}, \quad (11)$$

and the determinant of J is 1, i.e., the map is volume-preserving. The same reasoning applies to an “upper-triangular layer” of the form

$$x \mapsto x + \sigma(Ux + b). \quad (12)$$

In practice we combine many of those layers where the activation function is either (i) a fixed nonlinearity (tanh in our case) or (ii) identity. This is shown in Figure 2.

4 Volume-preserving transformer

In this section we introduce a new attention mechanism that we call *volume-preserving attention*, which is strongly inspired by traditional *multi-step methods* [27]. To this end, we first have to define what volume preservation means for the product space

$$\times_T \mathbb{R}^d \equiv \underbrace{\mathbb{R}^d \times \cdots \times \mathbb{R}^d}_{T \text{ times}}. \quad (13)$$

Consider an isomorphism $\hat{\cdot}: \times_T \mathbb{R}^d \xrightarrow{\sim} \mathbb{R}^{dT}$ of the form:

$$Z = \begin{pmatrix} z_1^{(1)} & z_1^{(2)} & \cdots & z_1^{(T)} \\ z_2^{(1)} & z_2^{(2)} & \cdots & z_2^{(T)} \\ \cdots & \cdots & \cdots & \cdots \\ z_d^{(1)} & z_d^{(2)} & \cdots & z_d^{(T)} \end{pmatrix} \mapsto \begin{bmatrix} z_1^{(1)} \\ z_1^{(2)} \\ \cdots \\ z_1^{(T)} \\ z_2^{(1)} \\ \cdots \\ z_d^{(T)} \end{bmatrix} =: Z_{\text{vec}}. \quad (14)$$

We refer to the inverse of $Z \mapsto \hat{Z}$ as $Y \mapsto \tilde{Y}$. In the following we also write $\hat{\varphi}$ for the mapping $\hat{\varphi} = \tilde{\varphi} \circ \varphi \circ \hat{\cdot}$.

Definition 1 A mapping $\varphi : \times_T \mathbb{R}^d \rightarrow \times_T \mathbb{R}^d$ is said to be volume-preserving if the associated $\hat{\varphi}$ is volume-preserving.

The main difficulty in adapting a transformer-like architecture to be volume-preserving is to adapt the activation function. Indeed, the softmax acts vector-wise and cannot preserve volume. We thus replace the softmax by a different activation function, which is based on the Cayley transform:

$$\sigma(Y) = \text{Cayley}(Y) = (\mathbb{I}_T - Y)(\mathbb{I}_T + Y)^{-1}. \quad (15)$$

The Cayley transform maps skew-symmetric matrices to orthogonal matrices⁷. This results in a new activation function for the attention mechanism which we denote by $\Lambda(Z) = \sigma(Z^T A Z)$. Further note that the input into the Cayley transform has to be a skew-symmetric matrix. For this reason we need to constrain A to be also skew-symmetric. With this, $\Lambda(Z)$ is an orthogonal matrix and the entire mapping is equivalent to a multiplication by an orthogonal matrix in the *vector representation* shown in Equation (14). To see this, note that the attention layer performs the following operation:

$$Z \mapsto Z \Lambda(Z). \quad (16)$$

In the transformed coordinate system, that is in terms of the vector Z_{vec} defined in Equation (14), this is equivalent to multiplication by a block-diagonal matrix $\tilde{\Lambda}(Z)$ from the left:

$$\tilde{\Lambda}(Z) Z_{\text{vec}} := \begin{pmatrix} \Lambda(Z) & \mathbb{O} & \cdots & \mathbb{O} \\ \mathbb{O} & \Lambda(Z) & \cdots & \mathbb{O} \\ \cdots & \cdots & \ddots & \cdots \\ \mathbb{O} & \mathbb{O} & \cdots & \Lambda(Z) \end{pmatrix} \begin{bmatrix} z_1^{(1)} \\ z_1^{(2)} \\ \cdots \\ z_1^{(T)} \\ z_2^{(1)} \\ \cdots \\ z_d^{(T)} \end{bmatrix}. \quad (17)$$

It is easy to see that $\tilde{\Lambda}(Z)$ in Equation (17) is an orthogonal matrix.

While the replacement of the standard transformer attention with this new volume-preserving attention is the biggest change to the transformer architecture, in addition, the feedforward neural network is replaced by a volume-preserving feedforward network, and the first add connection is removed⁸. The resulting architecture is shown in Figure 3.

⁷The orthogonal matrices $\{B \in \mathbb{R}^{d \times d} : B^T B = \mathbb{I}_d\}$ form a Lie group under regular matrix multiplication. The associated Lie algebra is the vector space of skew-symmetric matrices $\mathfrak{g} = \{C : C + C^T = \mathbb{O}\}$ and the Lie algebra is mapped to the Lie group via the Cayley transform. More details on this can be found in e.g. [7].

⁸Removal of the add connection is necessary as the addition with the input is not a volume-preserving operation.

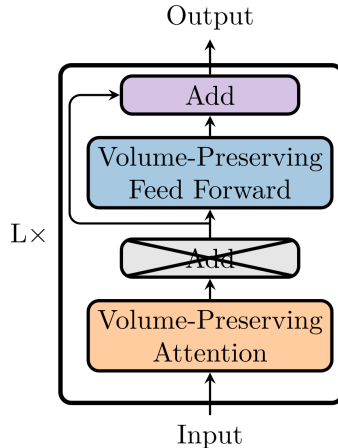


Figure 3: Architecture of the volume-preserving transformer. In comparison with the standard transformer in Figure 1, the Add layer has been removed, the attention layer has been replaced with a volume-preserving attention layer, and the feed forward layer has been replaced with the volume-preserving feedforward neural network from Figure 2.

5 Experimental results

In the following, we will consider the rigid body as an example to study the performance of our new volume-preserving transformer. We will solve the following equations (see Appendix A for the derivation):

$$\frac{d}{dt} \begin{bmatrix} z_1 \\ z_2 \\ z_3 \end{bmatrix} = \begin{bmatrix} Az_2z_3 \\ Bz_1z_3 \\ Cz_1z_2 \end{bmatrix}, \quad (18)$$

with $A = 1$, $B = -1/2$ and $C = -1/2$. We immediately see that the vector field Equation (18) is trivially divergence-free. In Figure 4, we show some trajectories.

We will compare three different neural network architectures that are trained on simulation data of the rigid body. These architectures are:

Architecture	Description	n.linear	n.blocks	L	Total number of parameters
VFFF	Volume-preserving feed-forward	1	6	-	135
VPT	Volume-preserving transformer	1	2	3	162
ST	Standard transformer	-	2	3	213

For the standard transformer, we further remove the optional add connection (i.e. the green line in Figure 1) to have a better comparison with the volume-preserving transformer which does not have an add connection. For the standard transformer, `n.blocks` refers to the number of ResNet layers we use (the last ResNet layer always has a linear activation).

5.1 Training data

As training data we take solutions of Equation (18) for various initial conditions:

$$\text{ics} = \left\{ \left(\begin{pmatrix} \sin(v) \\ 0 \\ \cos(v) \end{pmatrix}, \begin{pmatrix} 0 \\ \sin(v) \\ \cos(v) \end{pmatrix} : v \in 0.1 : 0.01 : 2\pi \right), \right. \quad (19)$$

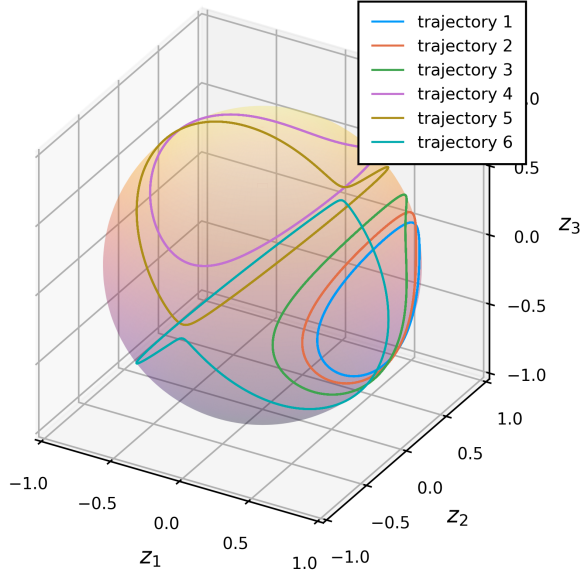


Figure 4: Rigid body trajectories for $A = 1$, $B = -1/2$ and $C = -1/2$ and different initial conditions.

where $v \in 0.1 : 0.01 : 2\pi$ means that we incrementally increase v from 0.1 to 2π by steps of size 0.01. We then integrate Equation (18) for the various initial conditions in Equation (19) with implicit midpoint for the interval $[0, 12]$ and a step size of 0.2. The integration is done with `GeometricIntegrators.jl` [28]. In Figure 4, we show some of the curves for the following initial conditions:

$$\left\{ \begin{pmatrix} \sin(1.1) \\ 0. \\ \cos(1.1) \end{pmatrix}, \begin{pmatrix} \sin(2.1) \\ 0. \\ \cos(2.1) \end{pmatrix}, \begin{pmatrix} \sin(2.2) \\ 0. \\ \cos(2.2) \end{pmatrix}, \begin{pmatrix} 0. \\ \sin(1.1) \\ \cos(1.1) \end{pmatrix}, \begin{pmatrix} 0. \\ \sin(1.5) \\ \cos(1.5) \end{pmatrix}, \begin{pmatrix} 0. \\ \sin(1.6) \\ \cos(1.6) \end{pmatrix} \right\}. \quad (20)$$

All solutions lie on a sphere of radius one.

5.2 Loss functions

For training the feedforward neural network and the transformer we pick similar loss functions. In both cases they take the form:

$$L_{\mathcal{NN}}(input, output) = \frac{\|output - \mathcal{NN}(input)\|_2}{\|output\|_2}, \quad (21)$$

where $\|\cdot\|_2$ is the L_2 -norm. The only difference between the two losses for the feedforward neural network and the transformer is that $input$ and $output$ are vectors $\in \mathbb{R}^d$ in the first case and matrices $\in \mathbb{R}^{d \times T}$ in the second.

5.3 Details on training and choice of hyperparameters

The code is implemented in Julia [29] as part of the library `GeometricMachineLearning.jl` [30]. All the computations performed here are done in single precision on an NVIDIA Geforce RTX 4090 GPU [31]. We use `CUDA.jl` [32] to perform computations on the GPU.

We train the three networks for $5 \cdot 10^5$ epochs and use an Adam optimizer [33] with adaptive learning rate η :

$$\eta = \exp\left(\log\left(\frac{\eta_2}{\eta_1}\right) / \text{n_epochs}\right)^t \eta_1, \quad (22)$$

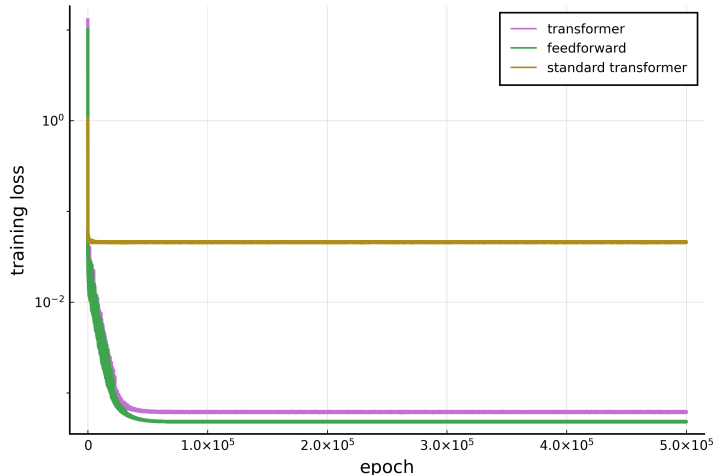


Figure 5: Training loss for the different networks.

where η_1 is the initial learning rate and η_2 is the final learning rate. We used the following values for the hyperparameters (mostly taken from [34]):

Name	η_1	η_2	ρ_1	ρ_2	δ	n_epochs
Value	10^{-2}	10^{-6}	0.9	0.99	10^{-8}	$5 \cdot 10^5$

With these settings we get the following training times (given as HOURS:MINUTES:SECONDS) for the different networks:

Architecture	VPPF	VPT	ST
Training time	4:02:09	5:58:57	3:58:06

The time evolution of the different training losses is shown in Figure 5. The training losses for the volume-preserving transformer and the volume-preserving feedforward neural network reach very low levels (about 5×10^{-4}), whereas the standard transformer is stuck at a rather high level (5×10^{-2}). The consequences are shown in Figure 6, where we plot the predicted trajectories for two initial conditions, $(\sin(1.1), 0, \cos(1.1))^T$ and $(0, \sin(1.1), \cos(1.1))^T$, for the time interval $[0, 100]$. These initial conditions are also shown in Figure 4 as “trajectory 1” and “trajectory 4”.

The standard transformer clearly fails on this task while the volume-preserving feedforward network slowly drifts of. The volume-preserving transformer shows much smaller errors and manages to stay close to the numerical solution. Figure 7 shows the time evolution of the relative error (compared to the solution with implicit midpoint) of the two volume-preserving networks.

5.4 Why does regular attention fail?

Figure 6 shows, that the standard transformer fails to predict the time evolution of the system correctly. The reason behind this could be that it is not sufficiently restrictive, i.e., the three columns making the output of the transformer (see Equation (6)) are not necessarily linearly independent; a property that the volume-preserving transformer has by construction. We observe that the “trajectory 1” and “trajectory 4” seem to merge at some point, as if there were some kind of attractor in the system. This is not a property of the physical system and seems to be mitigated if we use volume-preserving architectures.

5.5 A note on parameter-dependent equations

In the example presented here, training data was generated by varying the initial condition of the system, specifically

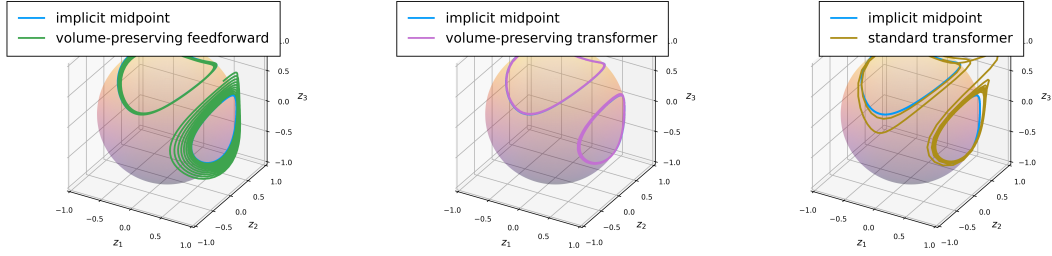


Figure 6: Sample trajectories of the rigid body obtained with the three neural networks: volume-preserving feedforward, volume-preserving transformer and the standard transformer, together with the numerical solution for “trajectory 1” and “trajectory 4” in Figure 4. The volume-preserving feedforward neural network is provided with the initial condition (i.e. $z^{(0)}$) and then starts the prediction and the two transformers are provided with the first three time steps ($z^{(1)}$ and $z^{(2)}$ are obtained via implicit midpoint) and then start the prediction. The prediction is made for the time interval $[0, 100]$, i.e. 500 time steps in total.

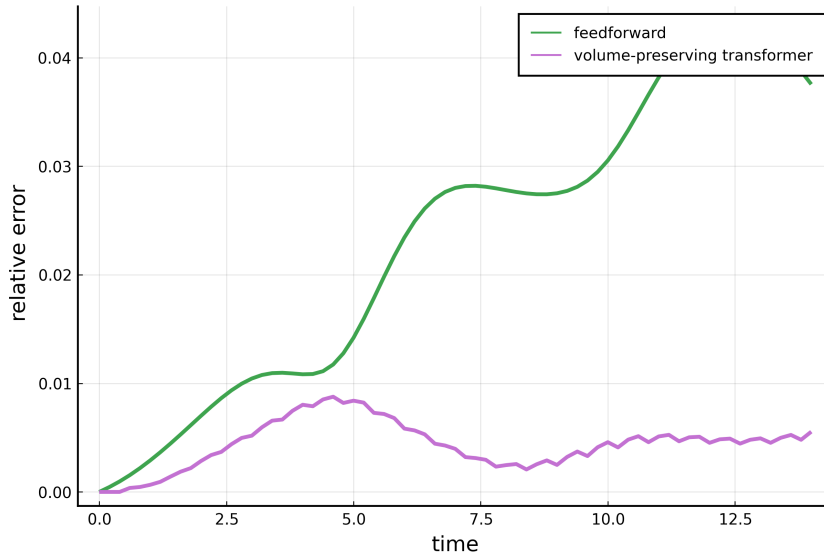


Figure 7: Comparison between the time evolution of the relative error of the volume-preserving feedforward neural network and the volume-preserving transformer.

$$\{\varphi^t(z_\alpha^0) : t \in (t_0, t_f], z_\alpha^0 \in \text{ics}\}, \quad (23)$$

where φ^t is the flow of the differential equation $\dot{z} = f(z)$, in particular the rigid body from Equation (18), t_0 is the initial time, t_f the final time, and ics denotes the set of initial conditions.

In applications such as *reduced order modeling* [12–14], one is often concerned with *parametric differential equations* of the form:

$$\dot{z} = f(z; \mu) \text{ for } \mu \in \mathbb{P}, \quad (24)$$

where \mathbb{P} is a set of parameters on which the differential equation depends. In the example of the rigid body, these parameters could be the moments of inertia (I_1, I_2, I_3) and thus the parameters (A, B, C) in Equation (18). A normal feedforward neural network is unable to learn such a parameter-dependent system as it *only sees one point at a time*:

$$\mathcal{NN}_{\text{ff}} : \mathbb{R}^d \rightarrow \mathbb{R}^d. \quad (25)$$

Thus a feedforward neural network can only approximate the flow of a differential equation with fixed parameters as the prediction becomes ambiguous in the case of data coming from solutions for different parameters. A transformer neural network⁹ on the other hand, is able to describe solutions with different parameters of the system, as it is able to *consider the history of the trajectory up to that point*.

6 Conclusion and future work

We have introduced a new neural network architecture, referred to as *volume-preserving transformer*, for learning the dynamics of systems described by divergence-free vector fields. This new architecture is based on the classical transformer, but modifies the attention mechanism, such that the resulting integrator is volume-preserving. We have shown that the new network leads to more accurate results than both the classical transformer and volume-preserving feedforward networks, when applied to volume-preserving dynamical systems, specifically the rigid body.

Future work will focus on the application of the new architecture to different systems and in particular parameter-dependent equations. A more thorough study of why and when classical attention fails (as was demonstrated in this work) is also desirable. Another interesting objective for future research is the proof of an universal approximation theorem for the volume-preserving feedforward neural network and perhaps even the transformer presented in this work. Efforts should also be directed towards making the learning process more efficient by reducing the number of epochs for small networks.

Acknowledgements.

We would like to thank the Centre International de Rencontres Mathématiques (CIRM) for their excellent hospitality that made this project possible. We further thank all participants of the Cemracs 2023 hackathon with who we had stimulating discussions as well as Léopold Trémant for suggesting the right output format of the transformer to us.

A The rigid body

In this appendix, we sketch the derivation of the rigid body equations used in Section 5. The differential equation for the rigid body [7, 8] describes the dynamics of a solid object fixed at a point. Figure 8

⁹It should be noted that recurrent neural networks such as LSTMs [5] are also able to do this.

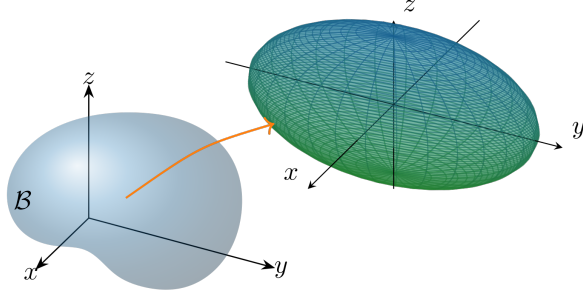


Figure 8: Any rigid body fixed at a point (left) can be described through an ellipsoid (right) through I_1 , I_2 and I_3 .

shows an example for a rigid body. Its dynamics can always be described in terms of an ellipsoid. To see this, let us consider the derivation of the rigid body equations. The motion of a point $(x_1, x_2, x_3)^T$ in the rigid body \mathcal{B} can be described as follows:

$$v := \frac{d}{dt} \begin{bmatrix} x_1 \\ x_2 \\ x_3 \end{bmatrix} = \omega \times \begin{bmatrix} x_1 \\ x_2 \\ x_3 \end{bmatrix} = \begin{pmatrix} \omega_2 x_3 - \omega_3 x_2 \\ \omega_3 x_1 - \omega_1 x_3 \\ \omega_1 x_2 - \omega_2 x_1 \end{pmatrix} = \begin{pmatrix} 0 & -\omega_3 & \omega_2 \\ \omega_3 & 0 & -\omega_1 \\ -\omega_2 & \omega_1 & 0 \end{pmatrix} \begin{bmatrix} x_1 \\ x_2 \\ x_3 \end{bmatrix}, \quad (26)$$

where ω is the angular velocity. The total kinetic energy of \mathcal{B} is obtained by integrating over the entire volume of the body:

$$T = \frac{1}{2} \int_{\mathcal{B}} \|v\|^2 dm = \frac{1}{2} \int_{\mathcal{B}} \|\omega \times x\|^2 dm = \frac{1}{2} \omega^T \Theta \omega, \quad (27)$$

where

$$\Theta_{ij} = \begin{cases} \int_{\mathcal{B}} (x_k^2 + x_\ell^2) dm & \text{if } i = j, \\ -\int_{\mathcal{B}} x_i x_j dm & \text{else,} \end{cases} \quad (28)$$

dm indicates an integral over the mass density of the rigid body, and $i \neq k \neq \ell \neq i$ for the first case.

The mathematical description of a rigid body (modulo rotations) does not require knowledge of the precise shape of the body. As Θ is a symmetric matrix, we can write the kinetic energy as:

$$T = \frac{1}{2} \omega^T \Theta \omega = \frac{1}{2} \omega^T U^T I U \omega, \quad (29)$$

with $I = \text{diag}(I_1, I_2, I_3)$. This shows that it is sufficient to know the eigenvalues of the matrix Θ which are called *moments of inertia* and denoted by I_k for $k = 1, 2, 3$. From this point of view every rigid body is equivalent to an ellipsoid.

A.1 Formulation of the equations of motion in the Euler-Poincaré framework

The dynamics of the rigid body can be described through a rotational matrix $Q(t)$, i.e. each point of the rigid body $x(0) \in \mathcal{B}$ can be described through $x(t) = Q(t)x(0)$ where $Q(t)^T Q(t) = \mathbb{I}$. We can therefore describe the evolution of the rigid body through a differential equation on the Lie group $G := \{Q \in \mathbb{R}^{d \times d} : Q^T Q = \mathbb{I}\}$. The associated tangent vector $\dot{Q} \in T_Q G$ can be mapped to the Lie algebra¹⁰ $\mathfrak{g} = T_{\mathbb{I}} G$ by:

$$W := \dot{Q} Q^T = \begin{pmatrix} 0 & -\omega_3 & \omega_2 \\ \omega_3 & 0 & -\omega_1 \\ -\omega_2 & \omega_1 & 0 \end{pmatrix} \in \mathfrak{g}. \quad (30)$$

As was indicated in equation Equation (30), the components of the skew-symmetric matrix W are equivalent to those of the angular velocity ω as can easily be checked:

$$\dot{x}(t) = \frac{d}{dt}Q(t)x(0) = \dot{Q}(t)x(0) = \dot{Q}(t)Q^T(t)x(t) = W(t)x(t) = \omega(t) \times x(t). \quad (31)$$

With this description, the kinetic energy can be written as:

$$T = \frac{1}{2} \text{tr}(WDW^T), \quad (32)$$

where D is a diagonal matrix¹¹ that satisfies $I_1 = d_2 + d_3$, $I_2 = d_3 + d_1$ and $I_3 = d_1 + d_2$. We now write $z := I^{-1}\omega$ and introduce the following notation:

$$\hat{z} = \begin{bmatrix} z_1 \\ z_2 \\ z_3 \end{bmatrix}^{\wedge} = \begin{bmatrix} \frac{\omega_1}{I_1} \\ \frac{\omega_2}{I_2} \\ \frac{\omega_3}{I_3} \end{bmatrix}^{\wedge} = \begin{pmatrix} 0 & -\frac{\omega_3}{I_3} & \frac{\omega_2}{I_2} \\ \frac{\omega_3}{I_3} & 0 & -\frac{\omega_1}{I_1} \\ -\frac{\omega_2}{I_2} & \frac{\omega_1}{I_1} & 0 \end{pmatrix}. \quad (33)$$

and obtain via the Euler-Poincaré equations¹² for Equation (32):

$$\widehat{I\dot{\omega}} = [\widehat{I\omega}, W], \quad (34)$$

or equivalently:

$$\frac{d}{dt} \begin{bmatrix} z_1 \\ z_2 \\ z_3 \end{bmatrix} = \begin{bmatrix} Az_2z_3 \\ Bz_1z_3 \\ Cz_1z_2 \end{bmatrix}. \quad (35)$$

In the above equation, we defined $A := I_3^{-1} - I_2^{-1}$, $B := I_1^{-1} - I_3^{-1}$ and $C := I_2^{-1} - I_1^{-1}$. In all of the examples, we set $I_1 = 1$, $I_2 = 2$ and $I_3 = 2/3$, thus yielding $A = 1$, $B = -1/2$ and $C = -1/2$.

B References

- [1] N. Baker, F. Alexander, T. Bremer, A. Hagberg, Y. Kevrekidis, H. Najm, M. Parashar, A. Patra, J. Sethian, S. Wild and others. *Workshop report on basic research needs for scientific machine learning: Core technologies for artificial intelligence* (USDOE Office of Science (SC), Washington, DC, 2019).
- [2] B. Chen, K. Huang, S. Raghupathi, I. Chandratreya, Q. Du and H. Lipson. *Discovering state variables hidden in experimental data*, arXiv preprint arXiv:2112.10755 (2021).
- [3] P. Goyal and P. Benner. *LQResNet: a deep neural network architecture for learning dynamic processes*, arXiv preprint arXiv:2103.02249 (2021).
- [4] A. Vaswani, N. Shazeer, N. Parmar, J. Uszkoreit, L. Jones, A. N. Gomez, L. Kaiser and I. Polosukhin. *Attention is all you need*. Advances in neural information processing systems **30** (2017).
- [5] S. Hochreiter and J. Schmidhuber. *Long short-term memory*. Neural computation **9**, 1735–1780 (1997).

¹⁰This is the Lie algebra of skew-symmetric matrices: $\mathfrak{g} = \{W \in \mathbb{R}^{d \times d} : W^T = -W\}$.

¹¹This matrix is equivalent to the diagonal entries of the *coefficient of inertia matrix* in [35].

¹²For the Euler-Poincaré equations we have to compute variations of Equation (32) with respect to $\delta W = \delta(\dot{Q}Q^{-1} = \dot{\Sigma} - [W, \Sigma])$ where $\Sigma := \delta QQ^{-1}$. For more details on this see [35].

- [6] A. Dosovitskiy, L. Beyer, A. Kolesnikov, D. Weissenborn, X. Zhai, T. Unterthiner, M. Dehghani, M. Minderer, G. Heigold, S. Gelly and others. *An image is worth 16x16 words: Transformers for image recognition at scale*, arXiv preprint arXiv:2010.11929 (2020).
- [7] E. Hairer, C. Lubich and G. Wanner. *Geometric Numerical integration: structure-preserving algorithms for ordinary differential equations* (Springer, Heidelberg, 2006).
- [8] V. I. Arnold. *Mathematical Methods of Classical Mechanics. Graduate Texts in Mathematics* (Springer, New York City, 1978).
- [9] M. Raissi, P. Perdikaris and G. E. Karniadakis. *Physics-informed neural networks: A deep learning framework for solving forward and inverse problems involving nonlinear partial differential equations*. Journal of Computational physics **378**, 686–707 (2019).
- [10] P. Jin, Z. Zhang, A. Zhu, Y. Tang and G. E. Karniadakis. *SympNets: Intrinsic structure-preserving symplectic networks for identifying Hamiltonian systems*. Neural Networks **132**, 166–179 (2020).
- [11] P. Buchfink, S. Glas and B. Haasdonk. *Symplectic Model Reduction of Hamiltonian Systems on Nonlinear Manifolds and Approximation with Weakly Symplectic Autoencoder*. SIAM Journal on Scientific Computing **45**, A289–A311 (2023).
- [12] T. Lassila, A. Manzoni, A. Quarteroni and G. Rozza. *Model order reduction in fluid dynamics: challenges and perspectives*. Reduced Order Methods for modeling and computational reduction, 235–273 (2014).
- [13] K. Lee and K. T. Carlberg. *Model reduction of dynamical systems on nonlinear manifolds using deep convolutional autoencoders*. Journal of Computational Physics **404**, 108973 (2020).
- [14] S. Fresca, L. Dede and A. Manzoni. *A comprehensive deep learning-based approach to reduced order modeling of nonlinear time-dependent parametrized PDEs*. Journal of Scientific Computing **87**, 1–36 (2021).
- [15] S. Chaturantabut and D. C. Sorensen. *Nonlinear model reduction via discrete empirical interpolation*. SIAM Journal on Scientific Computing **32**, 2737–2764 (2010).
- [16] A. Hemmasian and A. Barati Farimani. *Reduced-order modeling of fluid flows with transformers*. Physics of Fluids **35** (2023).
- [17] A. Solera-Rico, C. S. Vila, M. Gómez, Y. Wang, A. Almashjary, S. Dawson and R. Vinuesa, *β -Variational autoencoders and transformers for reduced-order modelling of fluid flows*, arXiv preprint arXiv:2304.03571 (2023).
- [18] J. Bajárs. *Locally-symplectic neural networks for learning volume-preserving dynamics*. Journal of Computational Physics **476**, 111911 (2023).
- [19] F. Kang and S. Zai-Jiu. *Volume-preserving algorithms for source-free dynamical systems*. Numerische Mathematik **71**, 451–463 (1995).
- [20] B. Leimkuhler and S. Reich. *Simulating hamiltonian dynamics* (Cambridge university press, Cambridge, UK, 2004).
- [21] S. Greydanus, M. Dzamba and J. Yosinski. *Hamiltonian neural networks*. Advances in neural information processing systems **32** (2019).
- [22] R. L. Bishop and S. I. Goldberg. *Tensor Analysis on Manifolds* (Dover Publications, Mineola, NY, 1980).
- [23] J. Achiam, S. Adler, S. Agarwal, L. Ahmad, I. Akkaya, F. L. Aleman, D. Almeida, J. Altschmidt, S. Altman, S. Anadkat and others. *Gpt-4 technical report*, arXiv preprint arXiv:2303.08774 (2023).
- [24] A. Graves and A. Graves. *Long short-term memory*. Supervised sequence labelling with recurrent neural networks, 37–45 (2012).
- [25] D. E. Rumelhart, G. E. Hinton, R. J. Williams and others. *Learning internal representations by error propagation* (1985).
- [26] K. He, X. Zhang, S. Ren and J. Sun. *Deep residual learning for image recognition*. In: *Proceedings of the IEEE conference on computer vision and pattern recognition* (2016); pp. 770–778.
- [27] K. Feng. *The step-transition operators for multi-step methods of ODE's*. Journal of Computational Mathematics, 193–202 (1998).
- [28] M. Kraus. *GeometricIntegrators.jl: Geometric Numerical Integration in Julia*, <https://github.com/JuliaGNI/GeometricIntegrators.jl> (2020).
- [29] J. Bezanson, A. Edelman, S. Karpinski and V. B. Shah. *Julia: A fresh approach to numerical computing*. SIAM review **59**, 65–98 (2017).

- [30] B. Brantner and M. Kraus. *GeometricMachineLearning.jl*, <https://github.com/JuliaGNI/GeometricMachineLearning.jl> (2020).
- [31] NVIDIA. *GeForce RTX 4090*, <https://www.nvidia.com/de-de/geforce/graphics-cards/40-series/rtx-4090/> (2022). Accessed on April 3, 2024.
- [32] T. Besard, C. Foket and B. De Sutter. *Effective Extensible Programming: Unleashing Julia on GPUs*. *IEEE Transactions on Parallel and Distributed Systems* (2018), [arXiv:1712.03112](https://arxiv.org/abs/1712.03112) [cs.PL].
- [33] D. P. Kingma and J. Ba. *Adam: A method for stochastic optimization*, arXiv preprint [arXiv:1412.6980](https://arxiv.org/abs/1412.6980) (2014).
- [34] I. Goodfellow, Y. Bengio and A. Courville. *Deep learning* (MIT press, Cambridge, MA, 2016).
- [35] D. D. Holm, T. Schmah and C. Stoica. *Geometric mechanics and symmetry: from finite to infinite dimensions*. Vol. 12 (Oxford University Press, Oxford, UK, 2009).